Causes of cracking in the turbine housings of a turbocharger

Causas del agrietamiento en las carcasas de turbina de un turbocompresor

Duffus-Scott, A. B.*[a], Machado-Rodríguez, L. A.[b], Álvarez-García, E. A.[c] and Patiño-Carachure, C.[d]

[a] ROR Universidad Central "Marta Abreu" de Las Villas • ID 0000-0001-9959-5697
[b] ROR Universidad Central "Marta Abreu" de Las Villas
[c] ROR Universidad Tecnológica de Campeche • LRC-9320-2024 • ID 0000-0002-8046-0124
[d] ROR Universidad Autónoma del Carmen • AGZ-9935-2022 • ID 0000-0002-1436-1259 • 226327

CONAHCYT classification

Area: Engineering
Field: Engineering and Technology
Discipline: Materials Science and Technology
Sub-discipline: Metallurgy

Key Handbooks

In this chapter, the procedure to determine the failure cause of the cracking of a casing that was exposed during its operation to thermal shock and fatigue conditions is explained. The areas of materials science and mechanical engineering are fundamental to determine the necessary studies according to the conditions and variables to be studied for this type of problem. The fundamental cause of cracking in the casing is due to thermal shock and fatigue which promote cracking. The maximum stress amplitude encountered due to thermal shock exceeds the permissible design limits. This work has been carried out in collaboration with the Centro de Investigaciones de Soldadura (CIS), Facultad de Ingeniería Mecánica e Industrial. Universidad Central "Marta Abreu" de Las Villas, Santa Clara, Villa Clara, Cuba. The Technological University of Campeche, San Antonio, Cardenas, Ciudad Del Carmen, Campeche and the Autonomous University of Carmen, Cd del Carmen, Campeche, Mex.
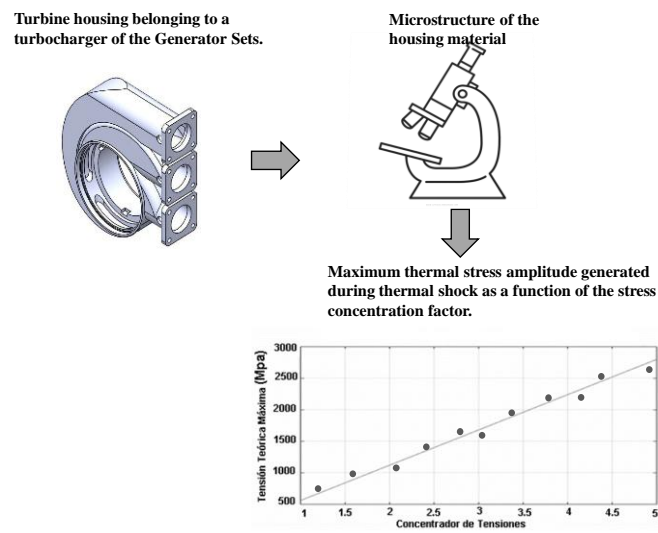
RENIECYT
Registro Nacional de Instituciones y Empresas Científicas y Tecnológicas
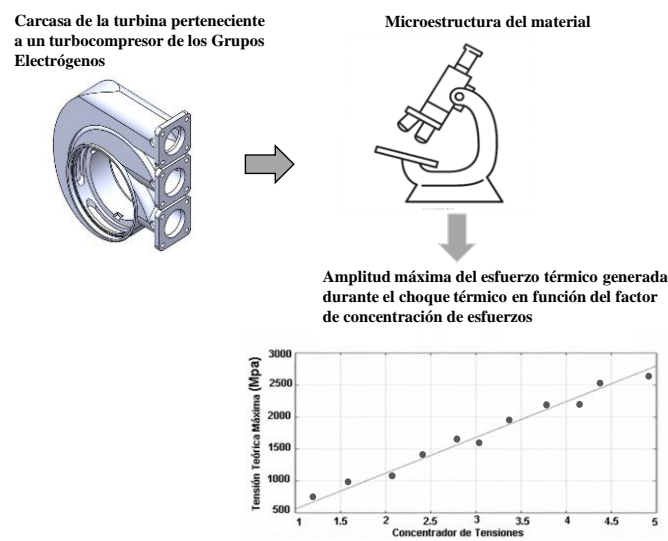1702902 CONAHCYT

Abstract

Temperature variation in turbocharger casings of generator sets generates shocks and thermal fatigue that cause cracks in different areas, with permissible limits depending on the direction and location. This study analyzes the microstructure and chemical composition of nodular cast iron castings manufactured under ASTM A 536 and GOST3443-87 standards, using metallographic techniques and emission spectroscopy. With visual inspection and penetrating liquids, the types of cracks and their orientations are examined. The maximum amplitude of the thermal stress generated during the thermal shock was determined using MATLAB software, considering that for a minimum stress concentration factor ($kf=1$), the thermal stress amplitude is 560 MPa, exceeding the design limit of 210 MPa, which explains the appearance of transverse and longitudinal cracks. Transverse cracks show a higher thermal stress concentration factor than longitudinal cracks.

Turbine housing belonging to a turbocharger of the Generator Sets.

Microstructure of the housing material

Maximum thermal stress amplitude generated during thermal shock as a function of the stress concentration factor.

Turbocharger, Cracking, Thermal shock

Resumen

La variación de temperatura en las carcasas de turbocompresores de grupos electrógenos genera choques y fatiga térmica que provocan grietas en diferentes zonas, con límites permisibles según la dirección y ubicación. Este estudio analiza la microestructura y composición química de las carcasas de hierro fundido nodular fabricadas bajo las normas ASTM A 536 y GOST3443-87, usando técnicas metalográficas y espectroscopía de emisión. Con inspección visual y líquidos penetrantes, se examinan los tipos de grietas y sus orientaciones. La amplitud máxima del esfuerzo térmico generada durante el choque térmico fue determinada con empleo del Software MATLAB, considerando que para un factor de concentración de esfuerzos mínimo ($kf=1$), la amplitud de tensión térmica es de 560 MPa, superando el límite de diseño de 210 MPa, lo cual explica la aparición de grietas transversales y longitudinales. Las grietas transversales muestran un mayor factor de concentración y esfuerzo térmico que las longitudinales

Carcasa de la turbina perteneciente a un turbocompresor de los Grupos Electrógenos

Microestructura del material

Amplitud máxima del esfuerzo térmico generada durante el choque térmico en función del factor de concentración de esfuerzos

Turbocompresor; Agrietamiento; Choque térmico

Introduction

The Fuel Generator Maintenance Company (Planned Preventive Maintenance: EMGEF, 2014) is currently in charge of the operation and maintenance of the Fuel-Oil Power Plants or Generator Sets. It carries out the technological operations for the disassembly, dismantling, inspection, maintenance and assembly of the TPS-57 turbocharger of HYUNDAIHIMSEN 9H 21/32 engines (Rodríguez, L. A.M., 2019).

According to Laustela, E. (2005), an exhaust gas turbocharger is driven, as the name suggests, by the engine exhaust gas. This gas, at high temperatures, is directed at high speed towards the blades of a turbine that drives a compressor rotor installed on the same shaft. As it rotates, the rotor draws in ambient air through a filter-silencer, compresses it and, through a aftercooler, sends it to the engine air intake, from where it passes into the cylinders. Turbocharging increases engine power by up to four times. Therefore, 75 per cent of the engine's power depends on the turbocharger working efficiently (Rodriguez, L.A.M., 2019).

The turbine is where the expansion of the gases coming from the engine cylinders takes place. The inlet of these gases is made through an orifice whose layout optimises the incidence of the flow on the blades, with this and the help of the snail-shaped housing (figure 1) the gases are distributed along the turbine losing pressure to make the shaft rotate. (Rodríguez, L.A.M. 2019).

Box 1

Figure 1
Turbine casing belonging to a turbocharger of the Generator Sets

Source*: Rodríguez L.A.M., 2019*

The casing is made of nodular cast iron, according to the ASTM A536 standard, which establishes 5 grades according to its mechanical properties; this standard is in correspondence with the GOST3443-87 standard.

According to Laustela, E. (2005), in Cuba there are cast iron casings with nodular and spheroidal graphite.

Nodular iron is a material currently widely used in the automotive industry and machinery, this is because it has some advantages over steel and grey iron, for example, it has greater resistance to fatigue and wear, although with a higher manufacturing cost than grey iron (García-Lira J., et al., 2019). Because of its good toughness, nodular iron is being used for the manufacture of parts that experience high fatigue cycles.

Shock often occurs when low temperature fluid hits a hot surface, producing a very high level of stresses close to the exposed surface that can eventually lead to the development of cracks, another less common situation in which thermal shock occurs can occur, particularly where sudden vessel depressurisation occurs (Mellouli, Haddar et al. 2011).

Based on the above, the aim of the present work is to chemically and metallographically characterise the casing material and to explain the causes of cracking in the casings of turbines belonging to turbochargers.

Methodology

Determination of the chemical composition of the casing material.

The chemical composition of the samples extracted from the casing was obtained by the method of Spectral Analysis of Optical Emission, which was carried out in the Chemical Analysis Laboratory of the Planta Mecánica Company, Cuba, with the use of an Optical Emission Spectral Analysis equipment, Belec Vario Lab Spectrograph (Figure 2), which processes the data with the Belec Win 21 software, the equipment's own. Prior to the analysis, the equipment was calibrated with the foundry standards.

Box 2

Figure 2

Optical emission spectral analysis equipment

Source: Spectrographer's Handbook, 2015

Metallographic observation

The material under study corresponds to a segment of a casing (see figure 1).

To prepare the specimens for metallographic analysis, samples were taken from a section of the carcass, by means of cuts on a metallographic cutting machine (Figure 3) in the Heat Treatment Laboratory of the Welding Research Centre.

Box 3

Figure 3

Metal cutting machine with abrasive disc

Source: *Own elaboration*

To facilitate handling during grinding and polishing, two samples were mounted on mechanical supports. The samples were prepared by grinding with sandpaper (from No 100 to No 1200) and polishing with alumina suspension, in accordance with ASTM E3-11 (2011). The grinding and polishing operations were performed on a metallographic polishing machine at the Heat Treatment Laboratory of the Welding Research Centre. After polishing, the samples were attacked with 3 % nital, in correspondence with ASTM E340-15 (2015) and ASTM E407-07(2015)e1 for micro attack.

The metallographic observation of the samples was carried out with the help of a Novel optical metallographic microscope at the Materials Science Laboratory of (CIS-MET-027, 2002). Images of the microstructure were taken with a high sensitivity 1.3 pixel Yuva camera attached to the eyepiece of the microscope and to a computer with specialised software (Image J) for image acquisition, as shown in Figure 4.
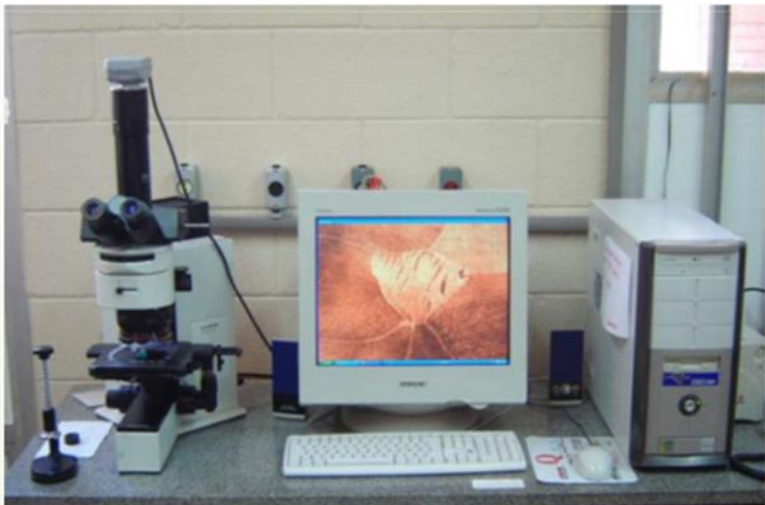
Box 4

Figure 4

Optical metallographic microscope, image acquisition camera and computer

Source: *Own elaboration*

Visual inspection and the application of liquid penetrants

Visual inspection and liquid penetrant testing were used as non-destructive testing methods for the analysis of the types of cracks that appear.

Developing the meaning of the variables in the linear and important writing is the comparison of the criteria used.

Determination of the maximum thermal stress amplitude generated during thermal shock.

The maximum thermal stress amplitude generated during thermal shock was determined using MatLab software. The maximum thermal stress amplitude generated during thermal shock (Sm) was determined by the equation (1) (ASME 2010):

$$S_m = \frac{E\alpha(\Delta T_m)}{2(1-v)} k_f \qquad [1]$$

S_m: is the maximum thermal stress amplitude generated during thermal shock.
E: is the modulus of elasticity
α : is the coefficient of thermal expansion.
ΔT_m: is the maximum possible magnitude of the thermal shock
v: is the Poisson coefficient
k_f: is the stress concentration factor with a value of 1,0 a 5,0.

Results

Chemical analysis

The results obtained from the chemical analysis are shown in table 1..

Box 5

Table 1

Chemical composition of the carcasses (% mass)

Material	C	Si	Mn	P	S	Mg	Cu	Cr	Al
Carcasa	4,4	1,9	0,19	0,018	0,007	0,008	0,017	0,014	--

Source: *Own elaboration*

This composition corresponds to the ASTM A536-84 (2019) e1 standard, which establishes 5 grades according to their mechanical properties (table 2).

Box 6

Table 2

Standard ASTM A536

Material	Code	Description	Uses general
ASTM A536	65-45-12	Mostly ferric; decoladaorecognised.	Components subjected to right-hand loads and fatigue.

Source: *Chiaverini, 1985*

The high carbon content in cast irons, both in the inclusion of graphite and the content in the matrix, is a factor that hinders the weldability of these materials (Guliaev, 1987, Aguilar et al ,2000).

The main alloying elements are carbon and silicon. High carbon content increases the amount of graphite or Fe3C and increasing the carbon and silicon content increases the graphitisation potential and fluidity of the cast iron, however, its strength is affected, as ferrite formation and pearlite thickening are promoted.

Analysis of metallographic observation

According to (Guliaev, A.P., 1987) cast irons can be classified as shown in figure 5.

Box 7

Figure 5

Classification of cast iron according to the structure of the metal matrix and the shape of the graphite inclusions.

Source: Guliaev, 1987

The following figures 6a and 6b at different magnifications show the type of melt and the matrix to which this material corresponds.
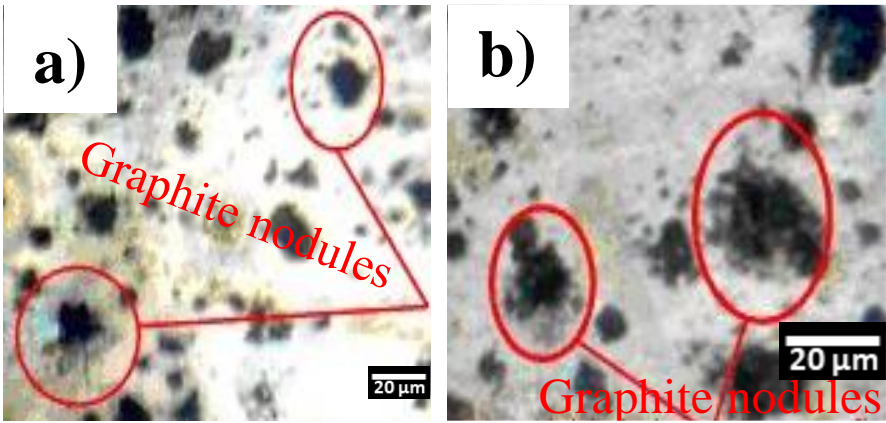
Box 8

Figure 6

Casing material microstructure (a- 200 X, b-400 X). CIS-MET-027

Source: *Own elaboration*

According to figure 6 it can be seen that the type of material present in the casing according to GOST 3443 - 87 is nodular cast iron (non-regular nodular inclusion shape), inclusion size 15-30 µm and uniform distribution of the ferritic matrix. This malleable cast iron, which is obtained by annealing (malleabelling) of white cast iron. In malleable cast iron, all or a large part of the carbon is in the free state in the form of nodules (carbonoderescent).

This compact, almost equiaxial shape of the graphite, but not round, is called nodular or annealed.

Results of the inspection of the casings

The visual inspection was based on detecting the different cracks in the casing, thus determining their length and the areas where they appear most frequently.

Several casings were inspected out of operation due to cracking and it was observed that the cracks appear more frequently in the transversal direction, being these the most dangerous as they cause a rapid breakage of the turbo and leakage of exhaust gases, which gives the lowest permissible value of length, this is explained because in the transverse direction the stress concentration factor (kf) is much higher. The following figure (figure 7) shows the different cracks that have occurred.
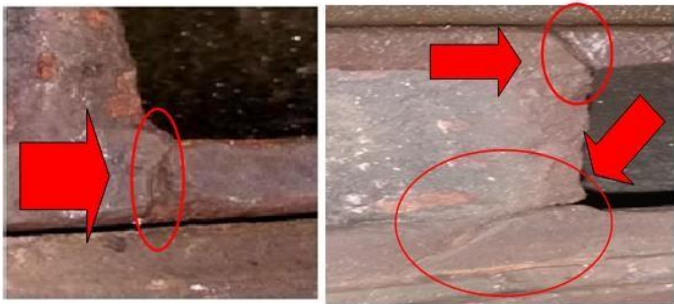
Box 9

Figure 7

Crack in the transverse direction

Source: own elaboration

Results of the determination of the thermal shock produced in the casing by MatLab software

For carbon steels with σúltima≤ 552 MPa, the allowable design stress amplitude (Sa) is considered to be in the order of 210 MPa (Callister. D.W., 2015).

According to (Callister D.W., 2015) the value of σultimate of nodular cast iron casing is of the order of 500MPa, this allows the same value of Sa= 210 MPa to be used.

The maximum possible amplitude of the thermal shock $DT_m= T_{carcasa}-T_{agua}$, where the

$T_{carcasa}= 380^0C$ and the $T_{agua}= 30^0C$, so that **$DT_m= 350^0C$.**

The stress concentration factor is decided to take values between 1 and 5 (ASME 2010).

The Poisson's coefficient **n= 0,25**, the coefficient of thermal expansion is **$a= 12*10^{-6} 1/^0C$** and the modulus of elasticity **$E= 2*10^5MPa$**. (Callister D.W., 2015)

The value of the maximum amplitude of the thermal stress generated during thermal shock (Sm) can be seen in the following graph (figure 8).
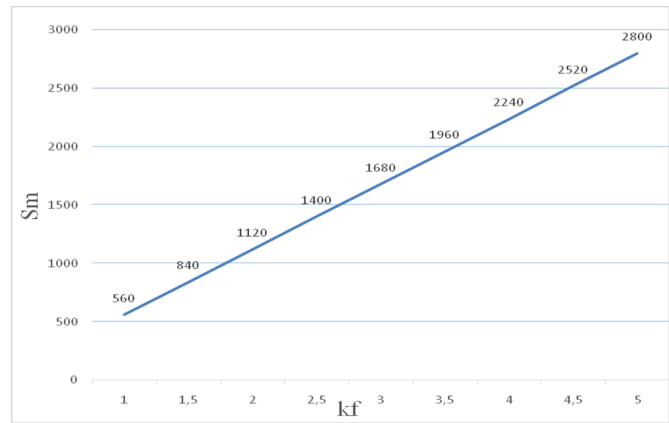
Box 10

Figure 8

Maximum thermal stress amplitude generated during thermal shock as a function of stress concentration factor

Source: own elaboration

The determination of the value of the maximum amplitude of the thermal stress generated during the thermal shock (Sm), is of great significance to have criteria about the appearance of cracks in the casing, if Sm is greater than Sa it implies that cracks will develop in the casing and due to the fact that the casing is subjected for intervals of time to this periodic stress, the cracks will propagate.

According to figure 5 for a stress concentrating factor (kf) of the order of 1, the value that reaches the maximum amplitude of the thermal stress generated during the thermal shock (Sm), is greater than Sa, therefore, this justifies the appearance of cracks both transversely and longitudinally.

Conclusions

The following conclusions have been drawn from the work:

Through the microstructural and chemical composition characterisation it was determined that the casing material corresponds to a cast iron with inclusion of nodular graphite and ferritic matrix.

The magnitude of the maximum amplitude of the thermal stress produced by the thermal shock generates cracks in the casing and due to the fact that the magnitude of this stress is also periodic, the phenomenon of thermal fatigue appears, bringing as a consequence the propagation of the cracks, i.e. the fundamental cause of the cracking in the casing is due to the thermal shock and thermal fatigue.

The maximum thermal stress amplitude generated during thermal shock (Sm), for the carcass under study, reaches a maximum value of 560 MPa for a stress concentration factor (kf=1).

As the magnitude of Sm (560 MPa) is much larger than Sa (210 MPa) and the carcass is periodically stressed, this justifies the crack propagation.

In the section of the shell where there is a higher stress concentration factor (kf), the probability of crack emergence is higher, due to the high stresses created in that area.

Conflict of interest

The authors declare that they have no conflicts of interest. They have no financial interests or personal relationships that could have influenced this book.

Authors' contribution

Patino-Carachure contributed to the writing analysis of the characterisation by optical microcopy,

Alvarez-García contributed to microstructural and metallographic analysis.

Duffus to microstructural and metallographic chemical analysis, PhD Machado to non-destructive testing.

Availability of data and materials

Data are available on request at: aduffus@uclv.edu.cu

Abbreviations

S_m: maximum thermal stress amplitude generated during thermal shock.
E: modulus of elasticity
a : coefficient of thermal expansion.
DT_m: maximum possible magnitude of thermal shock.
n: Poisson's coefficient
k_f: stress concentration factor

References

Background

García-Lira J., Castillo Sánchez M. D., Arenas Romero J. J. (2019). Benefits of austempered nodular iron (ADI) in the manufacture of parts. Memorias del Congreso Científico Tecnológico de las carreras de Ingeniería Mecánica Eléctrica, Industrial y Telecomunicaciones, sistemas y electrónica. YEAR 4. No. 4.

GOST3443 -87 (2005). Cast iron castings with graphite of different form. Methods of structure determination.

Laustela, E. (2005). The ABB turbocharger for increasing engine power and performance. ABB Magazine (3): 58-62.

Planned Preventive Maintenance. EMGEF. Technical paper, Santa Clara, (2014).

Mellouli, D., et al. (2011). 'Thermal fatigue of cast irons for automotive application.' Materials & Design 32(3): 1508-1514.

Rodriguez, L. A. M. (2019). Methodology for the reconditioning by welding of turbine casings of turbochargers of Generator Sets. Mechanical Engineering Project III, UCLV, Santa Clara, Villa Clara, Cuba.

Basic and support

Aguilar R. R.A, Celada E.R, Bonilla C. BJ. (2020). Weldability of grey iron, nodular iron and A304 stainless steel castings. Journal of the School of Graduate Studies, Vol. 11 No. 1.

ASME (2010). 'Rules for construction of Pressure Vessels.' An International Code VIII Division 2: 998.

ASTM E3-11 (2011). Standard Guide for Preparation of Metallographic Specimens.

ASTM E340-15 (2015). Standard practice for macroetching metals and alloys.

ASTM E407-07(2015)e1. Standard Practice for Microetching Metals and Alloys.

ASTM A536-84(2019)e1. Standard Specification for Ductile Iron Castings1.

CIS- MET-027, (2002). Procedure for observation of specimens by optical microscopy. Welding Research Centre (CIS-UCLV), Santa Clara.

Spectrograph Manual, Mechanical Plant, Santa Clara, Cuba, (2015).

Differences

Callister. D. W. (2015). 'Introduction to Materials Science and Engineering'. Department of Materials Science and Emgineering the University of Utah." Editorial Reverté, S.A.

Guliaev, A.P. (1987). Metallography Volume 2, Russia Ed. MIR.